Macromolecules

ARTICLE

pubs.acs.org/Macromolecules

# Bicontinuous Block Copolymer Morphologies Produced by Interfacially Active, Thermally Stable Nanoparticles

Se Gyu Jang,[†] Bumjoon J. Kim,[‡] Craig J. Hawker,[*,†,§,∥] and Edward J. Kramer[*,†,§,⊥]

[†]Materials Research Laboratory, [§]Department of Materials, [∥]Department of Chemistry and Biochemistry, and [⊥]Department of Chemical Engineering, University of California, Santa Barbara, Santa Barbara, California 93106, United States

[‡]Department of Chemical and Biomolecular Engineering, Korea Advanced Institute of Science and Technology, Daejeon 305-701, Republic of Korea

Supporting Information

**ABSTRACT:** Polymeric bicontinuous morphologies were created by thermal annealing mixtures of poly(styrene-*b*-2-vinylpyridine) (PS-*b*-P2VP) block copolymers and stabilized Au-core/Pt-shell (Au−Pt) nanoparticles. These Au−Pt nanoparticles have a cross-linked polymeric shell to promote thermal stability and are designed to adsorb strongly to the interface of the PS-*b*-P2VP block copolymer due to the favorable interaction between P2VP block and the exterior of the cross-linked shell of the nanoparticle. The interfacial activity of these Au−Pt nanoparticles under thermal annealing conditions leads to decrease in domain size of the lamellar diblock copolymer. As nanoparticle volume fraction $\phi_p$ was increased, a transition from a lamellar to a bicontinuous morphology was observed. Significantly, the effect of these shell-cross-linked Au−Pt nanoparticles under thermal annealing conditions was similar to those of traditional polymer grafted Au nanoparticles under solvent annealing conditions reported previously. These results suggest a general strategy for producing bicontinuous block copolymer structures by thermal processing through judicious selection of polymeric ligands, nanoparticle core, and block copolymer.

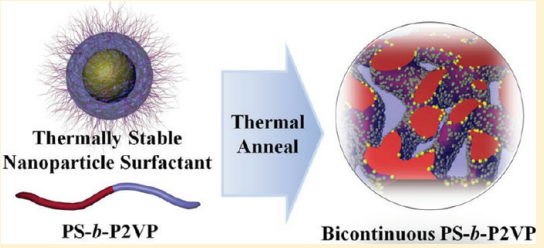


## 1. INTRODUCTION

Bicontinuous structures offer unique properties such as extremely high surface area and interconnectivity which provide opportunities to achieve higher efficiency in catalytic reaction, in charge carrier separation of photovoltaic films, and in transportation of molecular species such as ions through membranes for fuel cells and batteries.[1−6] Traditionally difficult to prepare, quenching of nonequilibrium structures in polymer blends,[7] stabilizing liquid/liquid phase separation with amphiphilic particles,[8,9] and top-down approaches such as holographic lithography and phase-mask lithography[10−13] have been reported to create bicontinuous structures. In contrast, self-assembly of block copolymers and surfactants has attracted significant interest due to its simple fabrication process, low cost, and ability to control domain sizes under 100 nm.[14−17] Various organic and inorganic mesoporous materials can be created from diblock copolymer templates, owing to the flexibility in choosing blocks from a broad library of polymers which allows the chemical/physical properties to be tuned. In addition, the availability of post-assembly infiltration of inorganic materials such as ceramics or noble metals provides novel function to the block copolymeric structures.[2,18] The main obstacle to this strategy is that the window of bicontinuous phases in phase diagrams of block copolymers is relatively narrow and block copolymers with different composition or molecular weights must be prepared in order to tune the size of the bicontinuous structure.[2,19,20] To resolve these problems, Kim et al. recently developed a novel method using interfacially active gold (Au) nanoparticles to modulate the interface of microphase-separated diblock copolymer domains resulting in formation of bicontinuous phases.[21,22] Significantly, bicontinuous phases were observed for various molecular weights of diblock copolymers, and the feature sizes of domains less than 100 nm were precisely controlled by the volume fraction of Au nanoparticles $\phi_p$.

The self-assembly of block copolymers into microphase-separated periodic structures has been intensively studied and attracted a great deal of attention in a variety of materials science fields such as catalysis, chemical sensing, photonic band gap modulation, and electronic device fabrication.[1,23−26] The annealing process to induce spontaneous self-assembly of block copolymers is a key step to allow microphase separation of distinct domains. Thermal annealing of block copolymers over the glass transition temperature ($T_g$) to provide mobility to the polymer chains has been widely used in both fundamental studies as well as applications of block copolymer self-assembly to obtain equilibrium morphology.[27,28] Meanwhile, solvent-assisted annealing of block copolymers has been mainly used to overcome drawbacks of the thermal annealing method. By the solvent annealing method, long-range ordering due to high mobility of polymer chains in solvent, control of self-assembly orientation by

**Received:** August 24, 2011
**Revised:** October 14, 2011
**Published:** November 11, 2011

establishing a solvent concentration gradient through the film, and capturing of metastable morphologies by rapid solvent drying has been achieved.[29−33] In addition, the use of solvent at room temperature as a plasticizer to reduce $T_g$ instead of thermal heating above $T_g$ allows studies on coassembly of block copolymers and noble metal nanoparticles. This overcomes the limit of thermal instability of metal−sulfur bond which causes detachment of polymer ligands and the corresponding destabilization of nanoparticles in the polymer matrix.[34−40] Despite the advantages of solvent annealing listed above, there are some issues to be considered. The physical properties of block copolymers, such as the Flory−Huggins interaction parameter ($\chi$) and corresponding order−disorder transition, in the presence of solvent will be different than under thermal annealing conditions due to the screening of unfavorable interactions by solvent and selectivity of solvent to the blocks. This may lead to different thermodynamic behaviors of block copolymers and corresponding nonequilibrium localization of nanoparticles in the block copolymer matrix.[41] Although there is some literature about coassembly of nanoparticles and block copolymers under thermal annealing conditions,[42−44] the interfacial activity and morphology transitions induced by thermally stable nanoparticles under thermal annealing conditions have not been explored.

To significantly increase the versatility of interfacially active nanoparticles, we create here interpenetrating bicontinuous structures by thermal annealing composites of PS-*b*-P2VP block copolymers and thermally stable nanoparticles. Thermally stable shell-cross-linked Au-core/Pt-shell (Au−Pt) nanoparticles are synthesized by cross-linking pendant double bonds on the PI block of thiol-terminated poly(styrene-*b*-1,2&3,4 isoprene) (PS-*b*-PI-SH) ligands with 1,1,3,3-tetramethyldisiloxane (TMDS) under a hydrosilylation reaction condition.[45] Shell-cross-linked Au−Pt nanoparticles were stable in toluene at 130 °C for 24 h, and no aggregation of nanoparticles was observed in a PS-*b*-P2VP diblock copolymer after annealing at 190 °C for 4 days.[45] It is noteworthy that our shell-cross-linking strategy can be generally applied to synthesize nanoparticles with various functional core materials requiring thermal processing. In direct contrast to prior work, thermal annealing of nanoparticles and block copolymers mixtures allows interfacial behavior of nanoparticles in the absence of any solvent effects to be investigated. In a PS-*b*-P2VP diblock copolymer matrix as a model system, the shell-cross-linked Au−Pt nanoparticles are strongly adsorbed to the interface of PS-*b*-P2VP due to the favorable interaction between the P2VP block and the cross-linked shell and lead to decreases in domain size and morphology transitions of these PS-*b*-P2VP block copolymers. The surfactant action of shell-cross-linked nanoparticles is directly compared with its solvent-annealed counterpart and shows similar interfacial behavior in these diblock copolymers. It is expected that the creation of bicontinuous structures via thermal annealing can be applied to the traditional polymer melt processing methods such as injection molding and extrusion.[46]

## 2. EXPERIMENTAL METHODS

**Synthesis of PS-*b*-PI-SH by Living Anionic Polymerization.** Thiol-terminated poly(styrene-*b*-1,2&3,4 isoprene) (PS-*b*-PI-SH) was synthesized by sequential anionic polymerization using tetrahydrofuran (THF) as a solvent at −78 °C as described elsewhere.[36] Briefly, styrene was initiated by *sec*-butyllithium and was polymerized for 3 h under argon. After 2 h, a small portion of polystyryl anion was taken with a gastight syringe to measure its molar mass by gel permeation chromatography (GPC) calibrated with PS standards. Then, isoprene was added at −78 °C and polymerized for 5 h under argon. The polyisoprenyl anions were then titrated with propylene sulfide, and the resulting polymers protonated by acidic methanol and stirred overnight. The number-average molecular weight $M_n$ values of the PS block was determined to be 3 kg/mol by GPC and that of the PI to be 1.4 kg/mol by end-group analysis using proton nuclear magnetic resonance spectroscopy ($^1$H NMR, Bruker, 500 MHz).

**Synthesis of PS-*b*-PI-Coated Au Nanoparticles.** Au nanoparticles coated with PS-*b*-PI-SH ligands (PS-*b*-PI-SAu) were synthesized via a two-phase toluene/water method using tetraoctylammonium bromide (TOAB, Sigma-Aldrich) as a phase transfer agent and sodium borohydride (Sigma-Aldrich) as a reducing agent.[47] The Au nanoparticles were precipitated in methanol at least three times to remove TOAB. The unbound polymer ligands were removed from the Au nanoparticles by precipitating the nanoparticles in hexane at least five times.

**Shell-Cross-Linking of PS-*b*-PI-Coated Au Nanoparticle.** Pendant double bonds within the PI block were cross-linked by a hydrosilylation reaction using 1,1,3,3-tetramethyldisiloxane (TMDS, Gelest Inc.) in the presence of chloroplatinic acid hexahydrate (CPA, Sigma-Aldrich).[45,48] First, the dry Au nanoparticle powder was dispersed in dry THF under argon. Subsequently, the Pt catalyst (100 mol %) and TMDS (150 mol % of Si−H groups) relative to pendant double bonds on the PI block dissolved in dry THF was added under magnetic stirring at room temperature. The dark red color of the Au nanoparticle dispersion turned dark brown after 30 min. The reaction continued for 2 days under argon. After the reaction was completed, nanoparticles were precipitated in a hexane and methanol mixture (1:1 v/v) at least three times. Hydrosilylation of the block copolymer PS-*b*-PI-SAu with pentamethyldisiloxane (PTMS) was conducted under the same experimental conditions.

**Preparation of PS-*b*-P2VP/Shell-Cross-Linked Au−Pt Nanoparticle Composites.** PS-*b*-PI-SAu or shell-cross-linked Au−Pt nanoparticles were dissolved in a freshly prepared solution in chloroform containing 1 wt % of a symmetric poly(styrene-*b*-2-vinylpyridine) block copolymer (PS-*b*-P2VP). The PS-*b*-P2VP block copolymers had number-average molecular weights $M_n$ of 114 kg/mol ($PS_{547}$-*b*-$P2VP_{543}$ where the subscripts are the average degrees of polymerization of the two blocks), 199 kg/mol ($PS_{979}$-*b*-$P2VP_{924}$), and 380 kg/mol ($PS_{1820}$-*b*-$P2VP_{1810}$, Polymer Source Inc.). The volume fraction of nanoparticles in the polymer/nanoparticle composite including the volume of polymer shell was estimated from the density of polymer (∼1.05 g/cm$^3$) and Au (∼19.3 g/cm$^3$) and by thermal gravimetric analysis (TGA) of the Au nanoparticles. Block copolymer/nanoparticle composites were prepared by drop-casting a solution of nanoparticles and PS-*b*-P2VP block copolymers in chloroform onto a Au-coated (∼100 nm thick) sodium chloride crystal window (Sigma-Aldrich, 2 mm thick). The composites were annealed under high vacuum (∼$10^{-8}$ Torr) at 190 °C for at least 3 days. For the composite sample of nanoparticles without a cross-linked shell, solvent annealing using saturated dichloromethane (DCM) vapor at room temperature for 2 days was employed. After annealing of the composite, a thick Au layer (∼100 nm) was deposited on the sample to inhibit infiltration of the epoxy resin (Embed-812, Electron Microscopy Sciences) into the sample during TEM sample preparation. Bulk samples of the composite were embedded into epoxy resin and sliced to a thickness of about 50−100 nm by ultramicrotoming. (Leica) The composite sample slices were exposed to iodine vapor to selectively stain the P2VP domains.

**Characterization.** The nanoparticles and cross-sectional images of composite samples were characterized by transmission electron microscopy (TEM, FEI Tecnai G2 microscope, 200 kV, and FEI Titan FEG for HR-TEM). The size histograms of the Au nanoparticles were

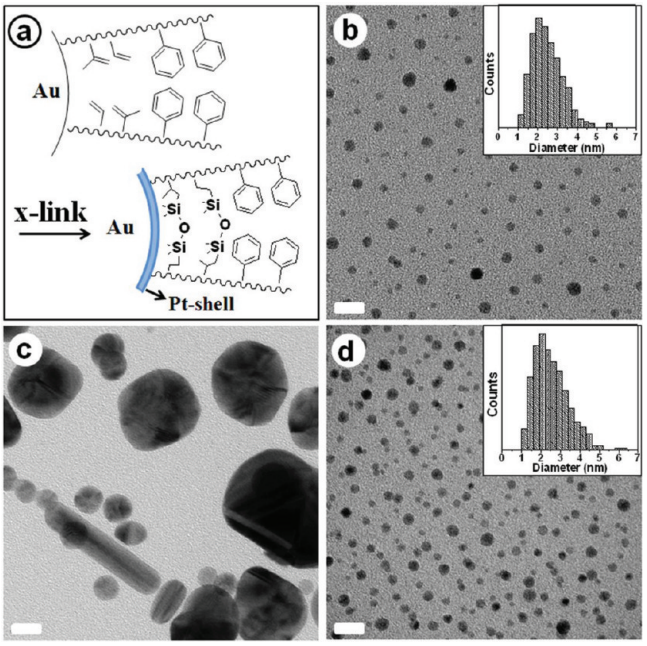


**Figure 1.** (a) A scheme illustrating the cross-linking of pendant double bonds on PI block of PS-*b*-PI ligands with TMDS in the presence of Pt catalyst. (b–d) TEM micrographs of Au and Au-core/Pt-shell (Au–Pt) nanoparticles. (b) Au nanoparticles with thiol-terminated PS-*b*-PI ligands before cross-linking of the PI block of the ligands. The areal chain density ($\Sigma$) of ligands on the Au-core surface, which was estimated from thermal gravimetric analysis (TGA) and $D_{av}$, was 1.7 chains/nm$^2$. (c) Au nanoparticles with un-cross-linked ligands after thermal treatment at 130 °C in toluene for 24 h. (d) Au–Pt nanoparticles after cross-linking of ligands followed by thermal treatment at 130 °C in toluene for 24 h. Scale bar is 10 nm in all cases. Inset histograms in (b) and (d) show the size distribution of the nanoparticles before and after thermal treatment, respectively.

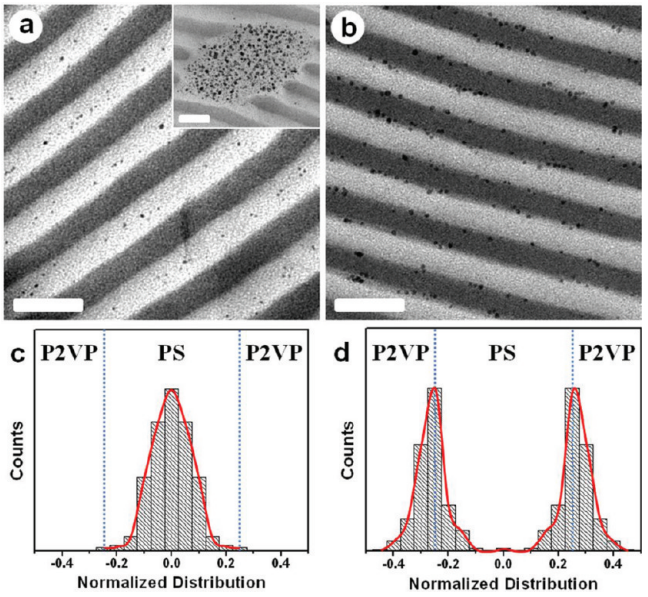


**Figure 2.** Effect of ligand-cross-linking on the localization of nanoparticles in a symmetric $PS_{547}$-*b*-$P2VP_{543}$ block copolymers ($M_n$ = 114 kg/mol). (a) Cross-sectional TEM micrograph of $PS_{547}$-*b*-$P2VP_{543}$ and Au nanoparticles with un-cross-linked ligands. The volume fraction ($\phi_p$) of nanoparticles is 0.05. The composite sample was solvent annealed at room temperature in dichloromethane vapor for 2 days. The P2VP domains appear as dark stripes after staining with iodine vapor. The nanoparticles (dark dots) are segregated to the PS domains (white stripes). Macrophase-separated Au nanoparticles were observed as shown in the inset. A histogram in (c) corresponding to the TEM micrograph in (a), obtained by image analysis of more than 300 nanoparticles, clearly shows the distribution of Au nanoparticles in the PS domains. The normalized distribution of nanoparticles plotted on the *x*-axis corresponds to the distance of nanoparticles from the center of the PS domain divided by the length of a single period of the structure formed by $PS_{547}$-*b*-$P2VP_{543}$, and the blue dotted lines located at +0.25 and −0.25 represent the interfaces between PS and P2VP. Extra care was taken by tilting the samples to align the direction of the lamellar planes and electron beam of the microscope to reduce the broadening of interfaces caused by misalignment of the electron beam. (b) Cross-sectional TEM micrograph of $PS_{547}$-*b*-$P2VP_{543}$ mixed with the shell-cross-linked Au–Pt nanoparticles ($\phi_p \sim 0.06$). The composite sample was annealed at 190 °C for 3 days under high vacuum ($\sim 10^{-8}$ Torr). The nanoparticles are segregated to the interface between PS and P2VP microdomains as shown in the TEM micrograph as well as in the histogram in (d). Scale bar in each micrograph is 50 nm.

determined from at least 300 nanoparticles by image analysis (Image Pro) of TEM micrographs. The mean areal chain density of polymer ligands on the Au nanoparticles was calculated from the total surface area and the weight fraction of Au and polymer ligands determined by TGA.

## 3. RESULTS

The diblock copolymer (PS-*b*-PI-SH) ligands on the Au nanoparticles containing the pendant double bonds on the PI block were cross-linked via hydrosilylation with 1,1,3,3-tetramethyldisiloxane (TMDS) in the presence of a platinum catalyst (Figure 1a). The Pt catalyst was reduced on the Au nanoparticles during the hydrosilylation reaction, resulting in the formation of a Pt shell on the Au nanoparticle (shell-cross-linked Au–Pt) as reported previously.[45] The formation of Pt shell and the effect of residual Pt catalyst in the cross-linked shell on the nanoparticles segregation in PS-*b*-P2VP diblock copolymer will be described later in the paper. Figure 1b is a transmission electron microscopy (TEM) image of Au nanoparticles (PS-*b*-PI-SAu) synthesized by the two-phase toluene/water method with the thiol-terminated diblock copolymer ligands of poly(styrene-*b*-1,2&3,4 isoprene) (PS-*b*-PI-SH). The molecular weights $M_n$s of PS and PI were about 3 and 1.4 kg/mol, respectively. The average diameter of nanoparticles ($D_{av}$) was 2.5 ± 0.8 nm as determined by image analysis of TEM micrographs. After thermal stability testing performed in a sealed ampule containing the PS-*b*-PI-SAu nanoparticles dissolved in toluene at 130 °C for a day, the PS-*b*-PI-SAu nanoparticles without a cross-linked shell that were still in solution had grown significantly in diameter as shown in Figure 1c with most PS-*b*-PI-SAu nanoparticles precipitating. This growth in size is due mainly to the dissociation of ligands from the Au surface caused by the thermal instability of Au–S bonds, which results in aggregation and growth of the nanoparticles. In contrast, the shell-cross-linked Au–Pt nanoparticles show excellent thermal stability even after the same thermal stability testing (Figure 1d). The difference in average diameter of shell-cross-linked Au–Pt nanoparticles before and after the thermal stability testing ($\Delta D$) was negligible ($D_{av,\ cross\text{-}linked}$ = 2.5 ± 0.9 nm). This result indicates that the intermolecularly cross-linked ligands on shell-cross-linked Au–Pt nanoparticles tightly cover the nanoparticle surface even under high-temperature conditions.

The localization of nanoparticles in a diblock copolymer can be precisely controlled by adjusting the surface chemical composition of such nanoparticles with grafted short polymer chains.[22,34,35,38,39,49−51] If there is significant interaction between the nanoparticle surface and one of diblock copolymers, i.e. the Au nanoparticle surface and poly(2-vinylpyridine) (P2VP) block of poly(styrene-*b*-2-vinylpyridine) (PS-*b*-P2VP), the areal chain density of the polymer ligands on the nanoparticles ($\Sigma$) plays an important role in determining segregation location of nanoparticles. Under solvent annealing conditions the PS-*b*-PI-SAu nanoparticles having a PS outer brush without a cross-linked shell ($\Sigma$ of 1.7 chains/nm$^2$) were segregated to the PS domain of a lamellar $PS_{547}$-*b*-$P2VP_{543}$ diblock copolymer (114 kg/mol) as seen in the TEM micrograph shown in Figure 2a. Nanoparticles are observed as small black dots, and the dark gray and white stripes correspond to the iodine-stained P2VP and PS domains, respectively. The composite sample in Figure 2a was annealed in saturated dichloromethane (DCM) vapor because the thermal annealing of PS-*b*-PI-SAu nanoparticles without cross-linking the PI portion of the ligands resulted in aggregation of nanoparticles. The histogram in Figure 2c clearly shows that the PS-*b*-PI-SAu nanoparticles are preferentially located near the center of PS domains. Macrophase-separated PS-*b*-PI-SAu nanoparticles were observed however even at the low nanoparticle volume fraction $\phi_p$ of 0.05 (TEM micrograph in the inset). In contrast, the shell-cross-linked Au−Pt nanoparticles were strongly adsorbed to the interface of the $PS_{547}$-*b*-$P2VP_{543}$ diblock copolymer after thermal annealing at 190 °C for 3 days as shown in TEM micrograph (Figure 2b). The corresponding histogram shows the distribution of nanoparticles in diblock copolymer domains (Figure 2d). No nanoparticle aggregates caused by macrophase separation of nanoparticles from the diblock copolymer domains were observed. The shell-cross-linked Au−Pt nanoparticles were strongly adsorbed to the interface of $PS_{547}$-*b*-$P2VP_{543}$ diblock copolymer, and the decrease in PS-P2VP interfacial tension caused by this segregation leads to an increase in the interfacial area and a corresponding decrease in lamellar thickness of the diblock copolymer. The half period of the lamellae of the composite sample in Figure 2b was only 92% of that of the $PS_{547}$-*b*-$P2VP_{543}$ diblock copolymer without addition of nanoparticles thermally annealed for the same time and temperature. This observation indicates that the Au−Pt nanoparticles are interfacially active enough to reduce the interfacial energy $\gamma_{PS\text{-}P2VP}$ between PS and P2VP. The reason for localization of nanoparticles at the interface will be discussed in a later section.

The decrease in domain size of PS-*b*-P2VP block copolymer as a result of nanoparticle addition indicates that further addition of nanoparticles may create more interfacial area and corresponding formation of a bicontinuous morphology of PS-*b*-P2VP. To examine the decrease in domain size and corresponding morphology transition according to the nanoparticle addition, $PS_{547}$-*b*-$P2VP_{543}$ composite samples mixed with various cross-linked Au−Pt nanoparticle volume fractions $\phi_p$ ranging from 0.06 to 0.28 were prepared by thermal annealing at 190 °C for 3 days. Figure 3a is the cross-sectional TEM micrograph of a composite sample containing shell-cross-linked Au−Pt nanoparticles with $\phi_p \sim 0.06$. At this $\phi_p$, the overall lamellar structure was preserved. However, the domains of $PS_{547}$-*b*-$P2VP_{543}$ were distorted due to the reduced bending modulus of the lamellar phase as a result of nanoparticle addition as predicted by Pryamitsyn and Ganesan.[52] In addition, segregation of nanoparticles to the grain boundaries and defects in the lamellar block copolymer structure was

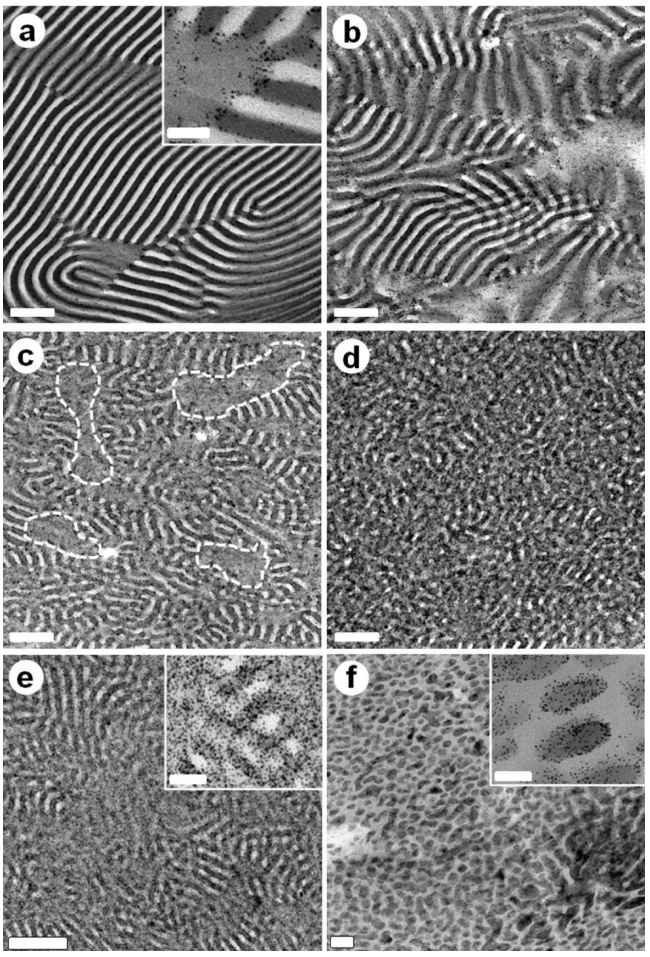


**Figure 3.** Cross-sectional TEM micrographs of thermally annealed (at 190 °C for 3 days) $PS_{547}$-*b*-$P2VP_{543}$ block copolymer films ($M_n$ = 114 kg/mol) mixed with various nanoparticle volume fractions $\phi_p$ of the Au−Pt nanoparticles after cross-linking of the ligands: (a) $\phi_p = 0.06$, (b) $\phi_p = 0.09$, (c) $\phi_p = 0.16$, and (d) $\phi_p = 0.28$. Lamellar structure of $PS_{547}$-*b*-$P2VP_{543}$ in (a) was gradually distorted and turned to a disordered bicontinuous phase as the volume fraction of nanoparticles is increased from (a) to (d). Scale bars from (a) to (d) are 200 nm. Cross-sectional TEM micrographs in (e) and (f) show as-cast mixture of diblock copolymers and nanoparticles prepared by drop-casting. (e) Morphology from the same solution used to obtain the bicontinuous phase in (d). (f) Morphology obtained from higher molecular weight $PS_{1820}$-*b*-$P2VP_{1810}$ (380 kg/mol, $\phi_p \sim 0.29$). P2VP block droplets associated with nanoparticles were observed rather than a lamellar morphology. Scale bars in (e) and (f) are 250 nm, and those in the inset images are 50 nm.

observed (TEM micrograph in the inset). This segregation may occur in order to minimize unfavorable block copolymer chain stretching.[37] The distortion of the lamellar domains is more pronounced as $\phi_p$ is increased as shown in Figures 3b ($\phi_p \sim 0.09$) and 3c ($\phi_p \sim 0.16$) with the normalized lamellar domain thickness $h(\phi_p)/h_0$, which is the ratio of lamellar domain thickness (half the lamellar period) $h(\phi_p)$ at a volume fraction $\phi_p$ to the lamellar domain thickness $h_0$ for $\phi_p = 0$, being reduced to ~0.82 (Figure 3b) and ~0.62 (Figure 3c). In Figure 3c, the transition of lamellar to a bicontinuous phase was incomplete as evidenced by the lamellar planes perpendicular to the viewing angle of TEM marked as dashed white circles. These lamellar planes disappeared, and the bicontinuous morphology was fully

developed at $\phi_P \sim 0.28$ as shown in Figure 3d ($h(\phi_P)/h_0 \sim 0.5$). Although the samples in Figure 3 have been characterized by only TEM, we believe that the morphology in Figure 3d is an interconnected bicontinuous morphology based both on its similarity to the morphology of previous solvent annealed samples and based on TEM micrographs (not shown) of the morphology taken with various tilt angles.

The composite samples described above were prepared by initially drop-casting a chloroform solution containing diblock copolymers and nanoparticles followed by thermal annealing to obtain equilibrium morphologies. Since chloroform evaporates rapidly at room temperature, there is the possibility that the bicontinuous morphology observed is a kinetically trapped nonequilibrium phase that cannot be altered by thermal annealing.[7] Figure 3e shows a representative cross-sectional TEM micrograph of an as-cast composite prepared from the same solution ($\phi_P \sim 0.28$) used to obtain the bicontinuous phase in Figure 3d. Although the interfaces between PS and P2VP domain are not clear, microphase-separated domains were observed. However, the overall morphology is similar to that of the composite sample in Figure 3c which is not fully bicontinuous. In addition, a significant number of Au−Pt nanoparticles are trapped in P2VP domains as shown in the inset. The morphology of an as-cast composite with a higher molecular weight PS-*b*-P2VP diblock copolymer (lamellar forming $PS_{1820}$-*b*-$P2VP_{1810}$, 380 kg/mol, $\phi_P \sim 0.29$) was also characterized as shown in Figure 3f. In contrast to the $PS_{547}$-*b*-$P2VP_{543}$, tiny P2VP droplets surrounded by, and containing, shell-cross-linked Au−Pt nanoparticles in a matrix of PS were observed rather than a lamellar or bicontinuous morphology. When thermally annealed at 190 °C for 3 days, the morphology of the $PS_{1820}$-*b*-$P2VP_{1810}$ with $\phi_P \sim 0.29$ is fully bicontinuous (TEM micrographs in the Supporting Information SF1). These observations indicate that the fully developed bicontinuous morphology, e.g., that shown in Figure 3d is an equilibrium state obtained by the interfacial action of surfactant-like shell-cross-linked Au−Pt nanoparticles rather than a state that has been kinetically trapped.

Having demonstrated the interfacial activity of thermally stable shell-cross-linked Au−Pt nanoparticles, their effect on lamellar-forming diblock copolymers with various molecular weights ranging from 114 to 380 kg/mol was explored by plotting $h(\phi_P)/h_0$ vs $\phi_P$ as shown in Figure 4 (solid lines with filled symbols). For a direct comparison, the interfacial activity of surfactant Au nanoparticles covered with a low areal chain density of short PS ligands in the same diblock copolymers but prepared by solvent annealing are also plotted as dotted lines with open symbols (data adopted from Kim et al.).[21] The shell-cross-linked Au−Pt nanoparticles in the PS-*b*-P2VP equilibrated under thermal annealing show interfacial activity that is qualitatively very similar to that of the Au surfactant nanoparticles with a low areal chain density of PS ligands in the diblock copolymers equilibrated by solvent annealing. In both cases, $h(\phi_P)/h_0$ was dramatically decreased by the addition of small volume fractions of nanoparticles with $h(\phi_P)/h_0$ being decreased more at the same $\phi_P$ for the higher molecular weight diblock copolymer. Moreover, in each case, bicontinuous morphologies were observed above a critical Au or Au−Pt nanoparticle volume fraction ($\phi_{P,c}$), where $\phi_{P,c}$ decreased as the molecular weight $M_n$ of the PS-*b*-P2VP diblock copolymer was increased. For the Au−Pt cross-linked shell nanoparticles $\phi_{P,c} \sim 0.28$ for $M_n$ = 114 kg/mol, 0.16 for $M_n$ = 199 kg/mol, and 0.09 for $M_n$ = 380 kg/mol. From these observations, it can be concluded that the formation of a bicontinuous phase is more highly dependent on the volume fraction of nanoparticles segregated to the interface than on the details of the annealing conditions, implying that both solvent annealing and thermal annealing can be used to obtain near equilibrium composite morphologies.

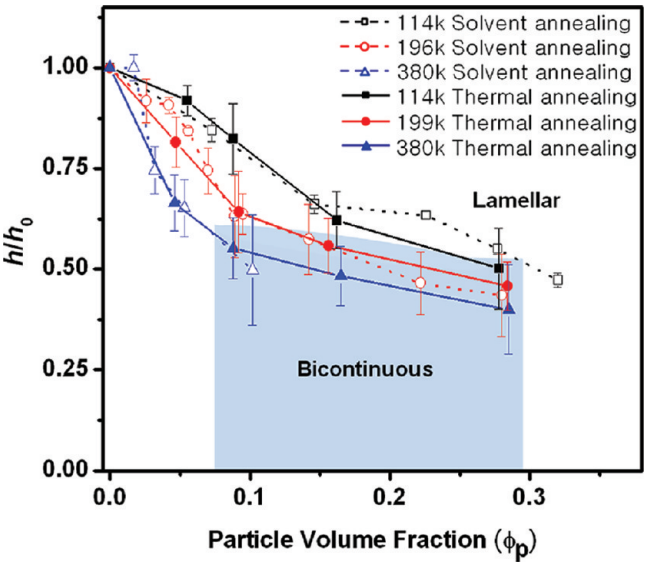


**Figure 4.** Phase diagram of PS-*b*-P2VP diblock copolymers plotted as normalized lamellar domain thickness vs nanoparticle volume fraction. Normalized lamellar domain thickness ($h(\phi_P)/h_0$) is the ratio of lamellar thickness as a result of addition of a nanoparticle volume faction $\phi_P$ ($h(\phi_P)$) to the thickness of the domain without addition of nanoparticles ($h_0$). A strong decrease in $h(\phi_P)/h_0$ was observed as $\phi_P$ is increased for all three different symmetric PS-*b*-P2VP diblock copolymers with various $M_n$ values of 114 kg/mol (solid black line with filled squares), 199 kg/mol (solid red line with filled circles), and 380 kg/mol (solid blue line with filled triangles). Bicontinuous morphologies of PS-*b*-P2VP were observed from the samples inside the shaded blue box. The $h(\phi_P)/h_0$ of solvent annealed composite samples plotted as a dotted black line with open squares (114 kg/mol), a dotted red line with open circles (199 kg/mol), and a dotted blue line with open triangle (380 kg/mol) are provided for comparison to the thermally annealed ones. The shell-cross-linked Au−Pt nanoparticles in the PS-*b*-P2VP equilibrated under thermal annealing show interfacial activity that is qualitatively very similar to that of the Au surfactant nanoparticles with a low areal chain density of PS ligands in the diblock copolymers equilibrated by solvent annealing.[21] Lines are drawn to guide the eye while symbols are experimental points.

## 4. DISCUSSION

Au nanoparticles covered with statistical random copolymer ligands of PS and P2VP (PS-*r*-P2VP-SH, PS molar fraction of 0.52) are reported to localize at the interface of and induce formation of a bicontinuous morphology in a high molecular weight PS-*b*-P2VP diblock copolymer ($M_n$ = 380 kg/mol) under solvent annealing conditions. In contrast, macrophase separation of these nanoparticles was observed when a shorter diblock copolymer was used ($M_n$ = 196 kg/mol).[21] These results imply that nanoparticles must have sufficiently strong attraction to block copolymer interfaces to avoid macrophase separation. A "neutral" random copolymer surface of the nanoparticle is not sufficient. The strong interfacial adsorption of Au nanoparticles with a low areal chain density of PS ligands caused by favorable

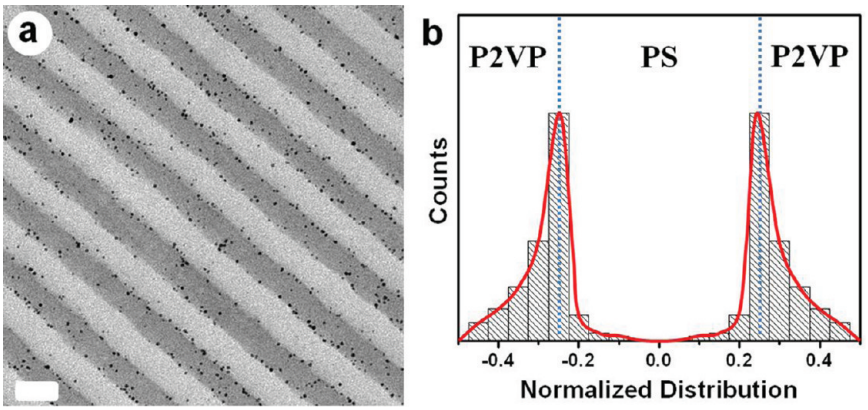


**Figure 5.** (a) TEM cross-sectional micrograph of a composite sample with lamellar-forming $PS_{979}$-*b*-$P2VP_{924}$ diblock copolymer (199 kg/mol) and PS-*b*-PI-SAu nanoparticles whose PI block ligands are decorated with pentamethyldisiloxane (PTMS) by the hydrosilylation reaction ($\phi_p \sim 0.09$). Scale bar is 50 nm. (b) Histogram showing the distribution of PTMS-decorated PS-*b*-PI-SAu nanoparticles in the $PS_{979}$-*b*-$P2VP_{924}$ diblock copolymer. The composite sample was annealed by saturated dichloromethane vapor for 2 days. Although the nanoparticles were mainly segregated at the interface similar to the Au−Pt nanoparticles shell-cross-linked by TMDS, a tail of the nanoparticle population in the P2VP domain was observed that is not present in the histogram in Figure 2d for the shell-cross-linked Au−Pt nanoparticles.

interaction between P2VP and the Au surface has been reported by Kim et al.[36,38] The partial coverage of Au surfaces by short polymer brushes with low $\Sigma$ ($<\Sigma_c$, the critical areal chain density) allows the Au surface to be exposed to P2VP due to rearrangement of mobile ligands on the surface of Au forming a "Janus" structure in contact with the interface.[49] In the present experiments bicontinuous morphologies of PS-*b*-P2VP of various molecular weights were created by shell-cross-linked Au−Pt nanoparticles segregated to the PS/P2VP interfaces with no macrophase separation of nanoparticles being observed even at $\phi_p \sim 0.28$, indicating a strong attraction between the shell-cross-linked Au−Pt nanoparticles and the PS/P2VP interface. The cross-linked network structure around the metal core however should prevent any rearrangement of that network structure to expose the metal core to the P2VP block.

If a favorable interaction between the nanoparticle cores and P2VP is blocked by the cross-linked shell, the enthalpic interaction between the diblock copolymer and the cross-linked shell itself may cause the shell-cross-linked Au−Pt nanoparticles to segregate to the interface of PS/P2VP. To examine this interaction, we consider the effective areal chain density ($\Sigma_{eff}$) at the surface of the cross-linked shell. $\Sigma_{eff}$ can be expressed as

$$\Sigma_{eff} = \Sigma\left(\frac{r_c}{r_{PI}}\right)^2$$

where $r_c$ and $r_{PI}$ are radii of Au−Pt core and PI shell, respectively. Because annealing of the composite was conducted under high vacuum ($10^{-8}$ Torr) without solvent, $r_{PI}$ can be easily calculated from the mass ratio of polymer to Au ($\sim$1.50 by TGA, measured before ligand cross-linking) as well as the density of PI (0.925 g/cm$^3$)[53] and Au (19.3 g/cm$^3$), together with the molecular weight ratio of PI to PS-*b*-PI-SH ($\sim$0.3). The estimated $\Sigma_{eff}$ of PS-*b*-PI-SAu cross-linked shell was about 0.4 chains/nm$^2$, which is significantly lower than the $\Sigma$ on the surface of Au−Pt core ($\sim$1.7 chains/nm$^2$) and, for this PS ligand molecular weight, well below the critical areal chain density ($\sim$1.6 chains/nm$^2$) needed to shield the cross-linked shell from the P2VP or PS.[37] Therefore, there can be a significant interaction between the outer surface of the cross-linked shell and both PS and P2VP blocks. The most likely cause of the strong interaction is residual Pt catalyst within the cross-linked shell after hydrosilylation. Although the residual Pt catalyst in the reaction solution was removed by precipitation, residual Pt in the cross-linked shell in the form of a Pt−vinyl and Pt−Si complexes was revealed by the XPS analysis of shell-cross-linked nanoparticles as detailed in the previous report[45] (see also XPS data and detailed discussion in the Supporting Information, Figure S2). A strong attraction between the P2VP block and the cross-linked shell containing residual Pt is possible due to the very low $\Sigma_{eff}$ of the PS brush and may result in the strong adsorption of shell-cross-linked nanoparticles to the PS/P2VP interface.

To confirm the presence of residual Pt and its effect on the localization of nanoparticles, double bonds in PS-*b*-PI-SAu nanoparticles were functionalized with monohydride pentamethyldisiloxane (PTMS) under the same hydrosilylation reaction conditions. The resulting nanoparticles should have very similar shell surface properties to the shell-cross-linked Au−Pt nanoparticle due to the similar chemical structure between TMDS and PTMS despite the absence of a cross-linked structure. The absence of cross-linking in the shell might be expected to allow greater penetration of P2VP block chains into the inner shell of PI when compared to the shell-cross-linked Au−Pt nanoparticles, resulting in increased interactions between P2VP and residual Pt. Figure 5a,b shows the cross-sectional TEM image and the distribution of PTMS-decorated Au−Pt nanoparticles in a $PS_{979}$-*b*-$P2VP_{924}$ diblock copolymer (199 kg/mol) that was prepared by solvent annealing ($\phi_p \sim 0.09$). The nanoparticles were mainly segregated to the interface like the shell-cross-linked Au−Pt nanoparticles. However, a significant tail of the nanoparticle distribution extends into the P2VP domain as shown in the histogram in Figure 5b; a similar tail is not observed for the shell-cross-linked Au−Pt nanoparticles in Figure 2d. Considering the fact that PS-*b*-PI-SAu nanoparticles were observed to be localized in PS domain as shown in Figure 2a, the higher population of the nanoparticles in P2VP domains can be rationalized by easier access of P2VP chains to the residual Pt in the non-cross-linked inner shell of PTMS decorated nanoparticles. Therefore, it is reasonable that adsorption of P2VP chains to residual Pt within the cross-linked PI shell with very low $\Sigma_{eff}$ localizes nanoparticles to the PS/P2VP interface.

## 5. CONCLUSION

Thermally stable, shell-cross-linked nanoparticles allowed us to explore the unknown effect of solvent in coassembly of nanoparticles and the diblock copolymer by comparing the surfactant actions of nanoparticles annealed by solvent and thermal heating. The shell-cross-linked nanoparticles were strongly adsorbed to the interface of PS-*b*-P2VP and induced a lamellar to bicontinuous morphological transition under thermal annealing. In both solvent and thermal annealing cases, a decrease in lamellar domain thickness of the diblock copolymer caused by a decrease in PS/P2VP interfacial tension leading to an increase in PS/P2VP interfacial area was observed as the nanoparticle volume fraction increased. The strong adsorption of the nanoparticles to the interfaces allowed bicontinuous morphologies of PS-*b*-P2VP with a broad range of molecular weights to be created by thermal annealing with no nanoparticle macrophase separation even at large volume fraction of nanoparticles. Compared to traditional solvent annealing strategies, the possibility of creating bicontinuous morphologies by thermal annealing adds significant processing flexibility including the prospect of producing bicontinuous block copolymer morphologies by standard melt processing methods such as extrusion. Furthermore, the flexibility of our shell-cross-linking strategy with various functional cores such as catalytic, magnetic, and fluorescent nanoparticles may provide opportunities to create multifunctional bicontinuous structures.

## ■ ASSOCIATED CONTENT

**Supporting Information.** Cross-sectional TEM micrographs of thermally annealed $PS_{1820}$-*b*-$P2VP_{1810}$ block copolymer films ($M_n$ = 380 kg/mol) mixed with shell-cross-linked Au−Pt nanoparticles (Figure S1); XPS data of shell-cross-linked Au−Pt nanoparticles and detailed discussion (Figure S2). This material is available free of charge via the Internet at http://pubs.acs.org.

## ■ AUTHOR INFORMATION

### Corresponding Author

*E-mail: hawker@mrl.ucsb.edu (C. J. H); edkramer@mrl.ucsb.edu (E.J.K.).

## ■ ACKNOWLEDGMENT

This work was supported primarily by the MRSEC Program of the National Science Foundation under Award DMR-1121053. S.G.J. was partially supported by a Korea Research Foundation Grant funded by the Korean Government [KRF-2008-357-D00050].

## ■ REFERENCES

(1) Jaramillo, T. F.; Baeck, S. H.; Cuenya, B. R.; McFarland, E. W. *J. Am. Chem. Soc.* **2003**, *125*, 7148.

(2) Crossland, E. J. W.; Kamperman, M.; Nedelcu, M.; Ducati, C.; Wiesner, U.; Smilgies, D. M.; Toombes, G. E. S.; Hillmyer, M. A.; Ludwigs, S.; Steiner, U.; Snaith, H. J. *Nano Lett.* **2009**, *9*, 2807.

(3) Wang, H.; Oey, C. C.; Djurisic, A. B.; Xie, M. H.; Leung, Y. H.; Man, K. K. Y.; Chan, W. K.; Pandey, A.; Nunzi, J. M.; Chui, P. C. *Appl. Phys. Lett.* **2005**, *87*, 023507.

(4) Hashimoto, T.; Tsutsumi, K.; Funaki, Y. *Langmuir* **1997**, *13*, 6869.

(5) (a) Ulbricht, M. *Polymer* **2006**, *47*, 2217. (b) Granick, S.; Kumar, S. K.; Amis, E. J.; Antonietti, M.; Balazs, A. C.; Chakraborty, A. K.; Grest, G. S.; Hawker, C. J.; Janmey, P.; Kramer, E. J.; Nuzzo, R.; Russell, T. P.; Safinya, C. R. *J. Polym. Sci., Part B: Polym. Phys.* **2003**, *41*, 2755–2793.

(6) Jones, B. H.; Lodge, T. P. *Chem. Mater.* **2010**, *22*, 1279.

(7) Aubert, J. H.; Clough, R. L. *Polymer* **1985**, *26*, 2047.

(8) Lee, M. N.; Mohraz, A. *Adv. Mater.* **2010**, *22*, 4836.

(9) Herzig, E. M.; White, K. A.; Schofield, A. B.; Poon, W. C. K.; Clegg, P. S. *Nature Mater.* **2007**, *6*, 966.

(10) Ullal, C. K.; Maldovan, M.; Wohlgemuth, M.; Thomas, E. L. *J. Opt. Soc. Am. A* **2003**, *20*, 948.

(11) Jin, W. M.; Shin, J. H.; Cho, C. Y.; Kang, J. H.; Park, J. H.; Moon, J. H. *ACS Appl. Mater. Interfaces* **2010**, *2*, 2970.

(12) Maldovan, M.; Ullal, C. K.; Jang, J. H.; Thomas, E. L. *Adv. Mater.* **2007**, *19*, 3809.

(13) Chan, T. Y. M.; Toader, O.; John, S. *Phys. Rev. E* **2006**, *73*, 046610.

(14) Bates, F. S.; Maurer, W. W.; Lipic, P. M.; Hillmyer, M. A.; Almdal, K.; Mortensen, K.; Fredrickson, G. H.; Lodge, T. P. *Phys. Rev. Lett.* **1997**, *79*, 849.

(15) Fleury, G.; Bates, F. S. *Soft Matter* **2010**, *6*, 2751.

(16) Pernot, H.; Baumert, M.; Court, F.; Leibler, L. *Nature Mater.* **2002**, *1*, 54.

(17) Falus, P.; Xiang, H.; Borthwick, M. A.; Russell, T. P.; Mochrie, S. G. J. *Phys. Rev. Lett.* **2004**, *93*, 145701.

(18) Hayward, R. C.; Chmelka, B. F.; Kramer, E. J. *Adv. Mater.* **2005**, *17*, 2591.

(19) Bates, F. S.; Fredrickson, G. H. *Annu. Rev. Phys. Chem.* **1990**, *41*, 525.

(20) Matsen, M. W.; Bates, F. S. *Macromolecules* **1996**, *29*, 1091.

(21) Kim, B. J.; Fredrickson, G. H.; Hawker, C. J.; Kramer, E. J. *Langmuir* **2007**, *23*, 7804.

(22) Kim, B. J.; Fredrickson, G. H.; Bang, J.; Hawker, C. J.; Kramer, E. J. *Macromolecules* **2009**, *42*, 6193.

(23) Bockstaller, M. R.; Thomas, E. L. *J. Phys. Chem. B* **2003**, *107*, 10017.

(24) Cheng, J. Y.; Ross, C. A.; Chan, V. Z. H.; Thomas, E. L.; Lammertink, R. G. H.; Vancso, G. J. *Adv. Mater.* **2001**, *13*, 1174.

(25) Mui, S. C.; Trapa, P. E.; Huang, B.; Soo, P. P.; Lozow, M. I.; Wang, T. C.; Cohen, R. E.; Mansour, A. N.; Mukerjee, S.; Mayes, A. M.; Sadoway, D. R. *J. Electrochem. Soc.* **2002**, *149*, A1610.

(26) Warren, S. C.; Messina, L. C.; Slaughter, L. S.; Kamperman, M.; Zhou, Q.; Gruner, S. M.; DiSalvo, F. J.; Wiesner, U. *Science* **2008**, *320*, 1748.

(27) (a) Fasolka, M. J.; Mayes, A. M. *Annu. Rev. Mater. Res.* **2001**, *31*, 323. (b) Oh, H.; Green, P. F. *Macromolecules* **2008**, *41*, 2561. (c) Oh, H.; Green, P. F. *Nature Mater.* **2009**, *8*, 139.

(28) Klok, H. A.; Lecommandoux, S. *Adv. Mater.* **2001**, *13*, 1217.

(29) (a) Lin, Z. Q.; Kim, D. H.; Wu, X. D.; Boosahda, L.; Stone, D.; LaRose, L.; Russell, T. P. *Adv. Mater.* **2002**, *14*, 1373. (b) Böker, A.; Lin, Y.; Chiapperini, K.; Horowitz, R.; Thompson, M.; Carreon, V.; Xu, T.; Abetz, C.; Skaff, H.; Dinsmore, A. D.; Emrick, T.; Russell, T. P. *Nature Mater.* **2004**, *3*, 302.

(30) Kim, S. H.; Misner, M. J.; Xu, T.; Kimura, M.; Russell, T. P. *Adv. Mater.* **2004**, *16*, 226.

(31) (a) Kimura, M.; Misner, M. J.; Xu, T.; Kim, S. H.; Russell, T. P. *Langmuir* **2003**, *19*, 9910. (b) Hu, Y.; Chen, D.; Park, S.; Emrick, T.; Russell, T. P. *Adv. Mater.* **2010**, *22*, 2583.

(32) Knoll, A.; Magerle, R.; Krausch, G. *J. Chem. Phys.* **2004**, *120*, 1105.

(33) Lodge, T. P.; Pudil, B.; Hanley, K. J. *Macromolecules* **2002**, *35*, 4707.

(34) Chiu, J. J.; Kim, B. J.; Kramer, E. J.; Pine, D. J. *J. Am. Chem. Soc.* **2005**, *127*, 5036.

(35) Kim, B. J.; Bang, J.; Hawker, C. J.; Kramer, E. J. *Macromolecules* **2006**, *39*, 4108.

(36) Kim, B. J.; Chiu, J. J.; Yi, G. R.; Pine, D. J.; Kramer, E. J. *Adv. Mater.* **2005**, *17*, 2618.

(37) Listak, J.; Bockstaller, M. R. *Macromolecules* **2006**, *39*, 5820.

(38) Kim, B. J.; Fredrickson, G. H.; Kramer, E. J. *Macromolecules* **2008**, *41*, 436.
(39) Park, S. C.; Kim, B. J.; Hawker, C. J.; Kramer, E. J.; Bang, J.; Ha, J. S. *Macromolecules* **2007**, *40*, 8119.
(40) Cheyne, R. B.; Moffitt, M. G. *Langmuir* **2005**, *21*, 10297.
(41) Huang, C. I.; Chapman, B. R.; Lodge, T. P.; Balsara, N. P. *Macromolecules* **1998**, *31*, 9384.
(42) Costanzo, P. J.; Beyer, F. L. *Macromolecules* **2007**, *40*, 3996.
(43) Lo, C. T.; Chao, C. J. *Langmuir* **2009**, *25*, 12865.
(44) Xu, C.; Ohno, K.; Ladmiral, V.; Milkie, D. E.; Kikkawa, J. M.; Composto, R. J. *Macromolecules* **2009**, *42*, 1219.
(45) Jang, S. G.; Khan, A.; Dimitriou, M. D.; Kim, B. J.; Lynd, N. A.; Kramer, E. J.; Hawker, C. J. *Soft Matter* **2011**, *7*, 6255.
(46) Rauwendaal, C. J. *Polymer Extrusion*, 4th ed.; Hanser Gardner Publications: Cincinnati, 2001.
(47) (a) Brust, M.; Walker, M.; Bethell, D.; Schiffrin, D. J.; Whyman, R. *J. Chem. Soc., Chem. Commun.* **1994**, 801. (b) van Berkel, K. Y.; Hawker, C. J. *J. Polym. Sci., Part A: Polym. Chem.* **2010**, *48*, 1594.
(48) Speier, J. L.; Webster, J. A.; Barnes, G. H. *J. Am. Chem. Soc.* **1957**, *79*, 974.
(49) Kim, B. J.; Bang, J.; Hawker, C. J.; Chiu, J. J.; Pine, D. J.; Jang, S. G.; Yang, S. M.; Kramer, E. J. *Langmuir* **2007**, *23*, 12693.
(50) Thompson, R. B.; Ginzburg, V. V.; Matsen, M. W.; Balazs, A. C. *Macromolecules* **2002**, *35*, 1060.
(51) Yeh, S. W.; Wei, K. H.; Sun, Y. S.; Jeng, U. S.; Liang, K. S. *Macromolecules* **2003**, *36*, 7903.
(52) Pryamitsyn, V.; Ganesan, V. *Macromolecules* **2006**, *39*, 8499.
(53) Hashimoto, T.; Shibayama, M.; Kawai, H. *Macromolecules* **1980**, *13*, 1237.